Hindawi Publishing Corporation
Journal of Nanomaterials
Volume 2008, Article ID 638947, 9 pages
doi:10.1155/2008/638947

Research Article

Nanomechanics of Single Crystalline Tungsten Nanowires

Volker Cimalla,[1] Claus-Christian Röhlig,[1] Jörg Pezoldt,[1] Merten Niebelschütz,[1] Oliver Ambacher,[1] Klemens Brückner,[1] Matthias Hein,[1] Jochen Weber,[2] Srdjan Milenkovic,[3] Andrew Jonathan Smith,[3] and Achim Walter Hassel[3]

[1] *Institut für Mikro- und Nanotechnologien, Technische Universität Ilmenau, Gustav-Kirchhoff-Strasse 7, 98693 Ilmenau, Germany*
[2] *Max-Planck-Institut für Festkörperforschung, HeisenbergStrasse 1, 70569 Stuttgart, Germany*
[3] *Max-Planck-Institut für Eisenforschung, Max-Planck-Strasse 1, 40237 Düsseldorf, Germany*

Correspondence should be addressed to Achim Walter Hassel, hassel@elchem.de

Received 2 September 2007; Accepted 29 January 2008

Recommended by Jun Lou

Single crystalline tungsten nanowires were prepared from directionally solidified NiAl-W alloys by a chemical release from the resulting binary phase material. Electron back scatter diffraction (EBSD) proves that they are single crystals having identical crystallographic orientation. Mechanical investigations such as bending tests, lateral force measurements, and mechanical resonance measurements were performed on 100–300 nm diameter wires. The wires could be either directly employed using micro tweezers, as a singly clamped nanowire or in a doubly clamped nanobridge. The mechanical tests exhibit a surprisingly high flexibility for such a brittle material resulting from the small dimensions. Force displacement measurements on singly clamped W nanowires by an AFM measurement allowed the determination of a Young's modulus of 332 GPa very close to the bulk value of 355 GPa. Doubly clamped W nanowires were employed as resonant oscillating nanowires in a magnetomotively driven resonator running at 117 kHz. The Young's modulus determined from this setup was found to be higher 450 GPa which is likely to be an artefact resulting from the shift of the resonance frequency by an additional mass loading.

1. INTRODUCTION

Tungsten is a brittle refractory metal that crystallises in the BCC form [1]. It has high-tensile strength and good creep resistance. However, it suffers from poor low-temperature ductility and strong reactivity in air [2]. Like the other BCC metals, tungsten also undergoes a brittle-to-ductile transition (BDTT) above 205°C. Below the BDTT it is very brittle exhibiting only few percents of elongation. The BDTT can only be lowered by heavy warm or cold deformation at temperatures below the room temperature. Due to its high stability this material is used in various applications in engineering. The trend for miniaturization of devices increases the demands for the selected materials to consider size effects of their properties. Most of the mechanical phenomena are well-known on a macroscopic scale, however, they are hard to determine on a nanoscopic scale. There is a variety of theoretical predictions of hardness and Young's modulus; mainly for carbon nanotubes [3], but only a few for nanowires (e.g., Au [4, 5]) which could not be confirmed experimentally up to date. Many metals are known to have oxidised surfaces under environmental conditions. This is also the case for tungsten, and the high surface to volume ratio in nanostructures amplifies the importance to consider this process [6]. Thus, a remarkable influence of the oxidised surface on the properties of the nanowires can be expected, which complicates the mechanical analysis of metal nanowires. Mechanical studies on nanowires are of interest as their diameter is already smaller than the average dislocation distance. The dislocations will therefore accumulate at the nanowires surface generating virtually dislocation free structures. These structures exhibit mechanical strength that may reach the theoretical limit. This is especially true if the wires are single crystalline [7]. Cutting of those structures from bulk material by means of a focused ion beam is one method to prepare the necessary test objects [8]. The FIB preparation often generates a large number of surface defects which limits the applicability of this method. Wang [9] has reviewed

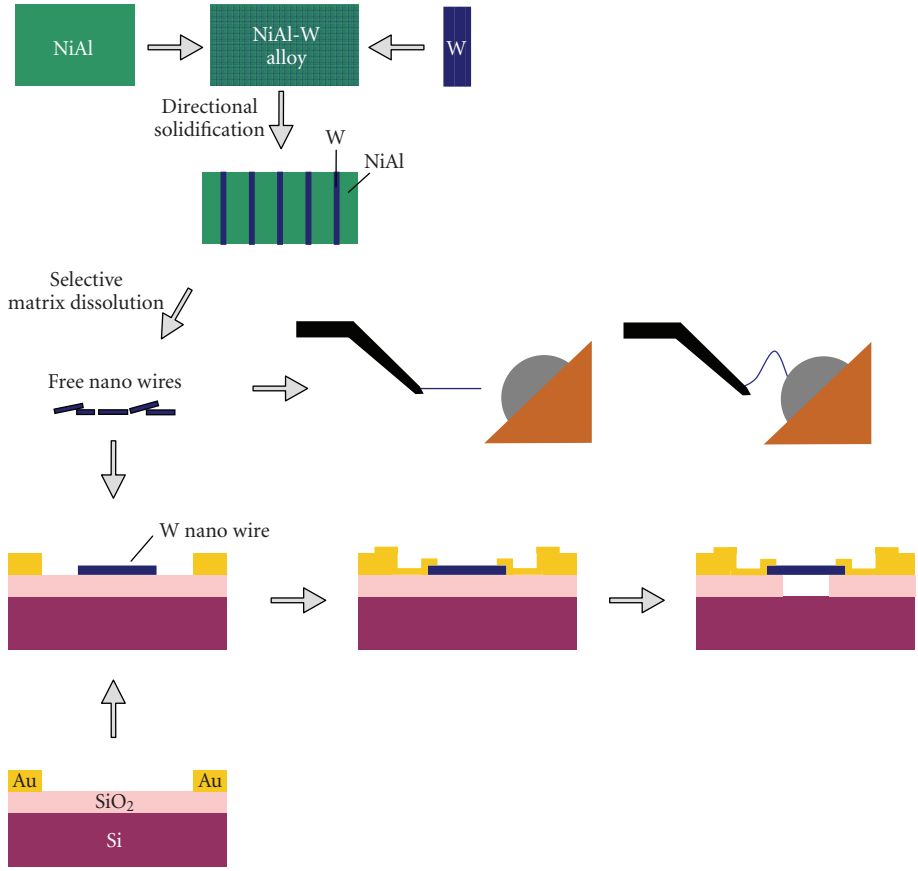

Figure 1: Roadmap of the processing steps employed in this work. A detailed description of the processing steps is given in the text.

the mechanical properties of nanowires and nanobelts characterised by techniques developed for mechanical characterisation using in situ transmission electron microscopy (TEM).

Recently, a method was established that allows producing single crystalline Re [10], W [11], Mo [12], Cu [13], and Au [14, 15] nanowires with a high-aspect ratio from directionally solidified eutectic alloys. By controlling the growth parameters and the dissolution conditions, the diameter [16] and the released length [15, 17], respectively, are well adjustable. The advantage of this system is that an array of nanowires is produced which allows studying the anisotropy of the mechanical properties. This was demonstrated for the Re system [18]. It is also possible to perform compression tests on Mo [19]. Since the release of the wires is done chemically or electrochemically, the surface of the wires is not mechanically affected, on the contrary deformations will be preferentially dissolved. This is well known and the reason why electropolishing is used for surface preparations for TEM samples.

The focus of this study lays in the investigation of stability and the mechanical properties of the tungsten nanowires. Different static and dynamic analysis approaches will be presented to extract one basic elastic property of the nanowires in comparison to the bulk material—the Young's modulus. The influence of the contamination and oxidation in air on the elastic behaviour is studied qualitatively in static bending experiments as well as in resonant oscillating nanomechanical devices.

2. EXPERIMENTAL

2.1. Preparation of the nanowires

The complete fabrication process from source material up to the mechanical test structure is schematically shown in Figure 1. The single steps are described in more detail in the following paragraph. Prealloys were prepared from nickel (99.97 wt%), electrolytic aluminium (99.9999 wt%), and tungsten (99.99 wt%) by induction melting under an inert atmosphere. They were drop cast into a cylindrical copper mould and subsequently fitted into alumina crucibles. Directional solidification was performedin a Bridgman-type crystal growing facility. The solidification was conducted at a temperature of $1700 \pm 10^{\circ}$C, a thermal gradient of approximately 40 K cm^{-1}, and a growth rate of 30 mm h^{-1}. Mechanical cutting and a standard metallographic preparation yielded the sample shown in Figure 2 in which the cross sections of the nanowires appear darker. This sample was further investigated by EBSD as discussed in the results section.

2.2. Nanowire release

In order to extract the tungsten wires from the matrix, the conditions under which both matrix elements—nickel and

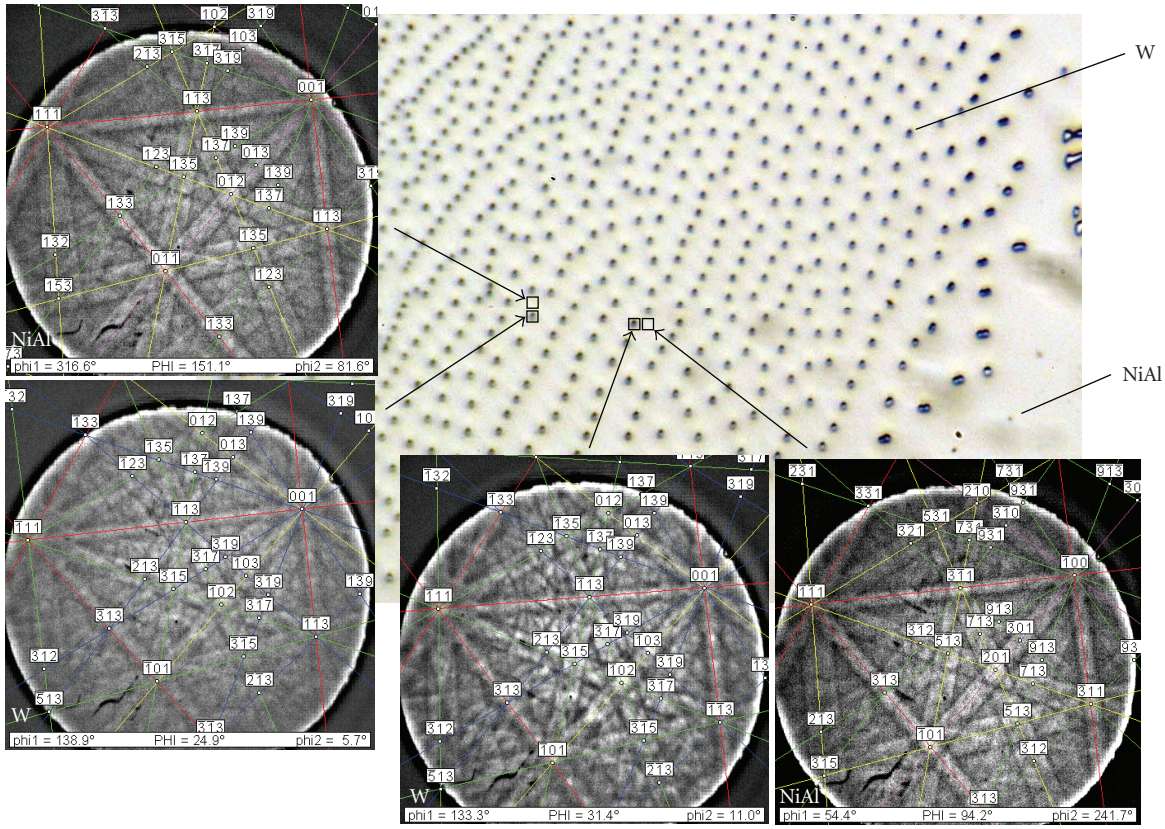

Figure 2: Optical image of a cross section through a directionally solidified NiAl-W eutectic. The W nanowires appear as darker spots in a bright NiAl matrix. Inserts: EBSD patterns at the marked positions with well-defined Kikuchi lines.

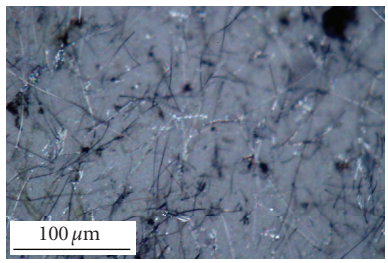

Figure 3: Bunch of tungsten nanowires on a filter paper with an approximate diameter of 200 nm, the tungsten nanowires become visible in an optical microscope due to the strong light scattering of the metal.

aluminium—corrode, while passivating tungsten was chosen, the details of which are described in [11]. Both a chemical and an electrochemical route are available to release these wires from the matrix. The chemical route pieces of the sample were immersed in a solution of HCl and H_2O_2 which leads to the selective digestion of the matrix phase [11]. The appropriate potential could also be applied electrochemically. By continuing the dissolution process for a few hours, the matrix was completely digested. In both cases, a subsequent filtration yielded free nanowires on a filter paper (see Figure 3). It clearly shows the extreme aspect ratio of these wires. All potentials in the electrolyte are given versus the standard hydrogen electrode (SHE). The chemicals were of p.a. grade and purchased from VWR, Germany.

2.3. Preparation of nanowires for mechanical investigation

For the processing of nanowire-based nanomechanical devices and test structures, no reliable technology for the large-scale fabrication exists and every structure can be considered as a handmade single device. Moreover, classical processes often damage or destroy bottom up nanomaterials [20]. In this work, two variants of a process technology were used, both bridging classical top down and novel bottom up methods.

The first method combines photolithography and electron-beam lithography as shown schematically in Figure 1. The basis is a silicon wafer with thermally grown SiO_2 and a matrix of large gold pads as well as alignment marks as in Figure 1. The pads are defined by photolithography and are used as interface between external wiring (bonding or attached tips) and the nanocontacts to the nanowires. The SiO_2 surface provides electrical isolation between the contacts and is also utilised to be etched by HF (hydrofluoric acid)-vapour-etching [21] to obtain freestanding nanowires.

The tungsten nanowires collected on filter paper (see Section 2.4) were transferred into a suspension of isopropanol or methanol after etching. After drying out on the substrate, the nanowires are randomly distributed on

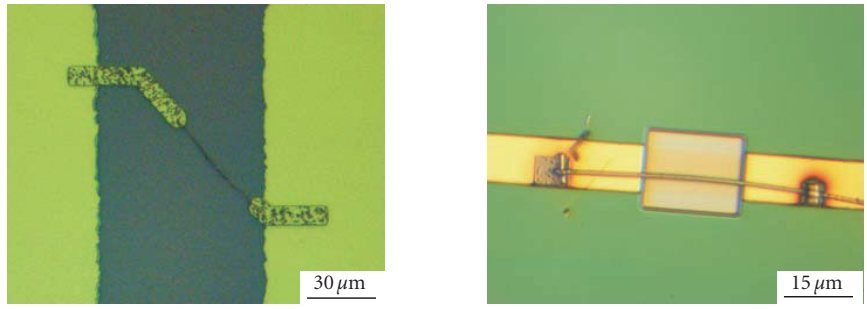

(a) (b)

Figure 4: Optical micrographs of contacted tungsten nanowires: (a) by electron beam lithography and (b) by FIB.

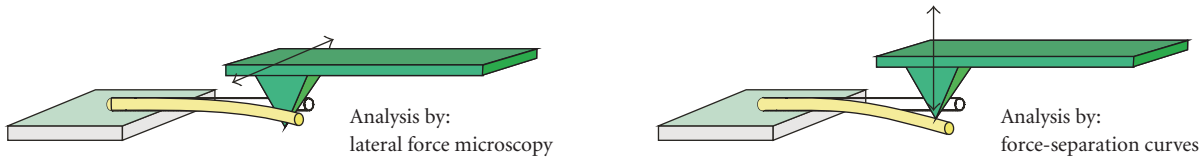

(a) (b)

Figure 5: Principles of static analysis of mechanical properties of nanowires by AFM.

the surface (Figure 1). Due to their light scattering properties, they can be localised in an optical microscope. Afterwards the position is mapped relative to the alignment marks, and the obtained coordinates are used to create a mask for the electrical contacts. The nanocontacts are prepared by e-beam lithography, Au evaporation, and lift off processing (Figure 1). A thin layer of chromium (Cr) is deposited first in order to improve the adhesion of gold on the SiO_2-surface.

Finally, the freestanding nanowires are realized by the undercut of the SiO_2. The sample is heated 13°C relative to the room temperature and is then placed into a chamber containing HF-vapour for 10 minutes (Figure 1). An example of a tungsten nanowire and the prepared Au nanocontacts is shown in Figure 4(a).

In a second method, nanowires can be contacted directly by writing the pads using Pt deposition by the focused ion beam (FIB) technique (see Figure 4(b)). A major disadvantage of the method is the possibility to contaminate the nanowires with Pt and carbon, which may alter the mechanical properties.

2.4. Chemical and structural characterisation

Chemical analysis of the solutions was performed by inductively-coupled plasma optical emission spectrometry (ICP-OES). Scanning electron microscopy was performed using a Leo 1550 VP apparatus (Leo Elektronenmikroskopie GmbH, Oberkochen, Germany) fitted with an INCA energy dispersive system (EDS) (Oxford Instruments, Oxford, UK).

A scanning electron microscope model JSM6500F from JEOL, Japan equipped with an EBSD detector from TSL was used for electron back scatter diffraction (EBSD) measurements. The patterns were recorded by a CCD camera (DigiView) 12 under a tilting angle of the sample stage of 70°. The acceleration voltage was 15 kV. The analysis of the individual EBSD patterns yielded the crystallographic orientations of the crystal at each position of the electron beam. In the present study, ACOM has been applied in a high-resolution, high-intensity SEM with field emission gun (JEOL JSM 6500 F). For pattern analysis, the TSL OIM analysis software was used.

2.5. Mechanical characterisation

2.5.1. Bending (static) experiments

Static bending experiments were performed on singly clamped nanowires by exposing a force on a nanowire clamped on one side only. As a qualitative test of mechanical properties of the tungsten nanowires, a micromanipulator was used for bending experiments, which were observed by optical microscopy. Quantitative analysis was performed using an atomic force microscope (AFM) in order to obtain the Young's modulus. This analysis was performed on laterally aligned nanowires (Figure 5).

2.5.2. Analysis of resonant oscillating nanowires

Dynamic studies can be performed on oscillating nanowires by analysis of the resonant frequency, which is given by the Euler-Bernoulli theory [22]:

$$f_{\text{res}} = \frac{\kappa^2}{2\pi l^2}\sqrt{\frac{EI}{\rho A}}, \tag{1}$$

with k being a constant depending on the oscillation mode. For the singly and doubly clamped oscillators (Figure 6), the

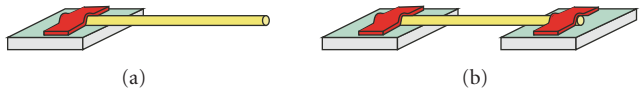

Figure 6: Basic configuration of nanowire-based resonators.

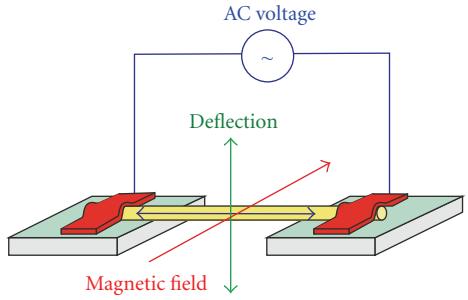

Figure 7: Magnetodynamic operation principle of doubly clamped nanowires with magnetomotive actuation and inductive sensing.

resonant frequency of the first flexural is then given by

$$f_{\text{res}} \approx 0.28\sqrt{\frac{E}{\rho}}\frac{R}{L^2}, \tag{2}$$

for singly clamped nanowires (cantilever), and

$$f_{\text{res}} \approx 1.78\sqrt{\frac{E}{\rho}}\frac{R}{L^2}, \tag{3}$$

for doubly clamped nanowires (bridge), with E being the Young's modulus and p the mass density of the resonator material, R and L are radius and length of the resonator beam, respectively. Consequently, resonators are powerful test structures for the determination of the Young's modulus on the nanoscale as long as the geometry can be determined accurately.

In this study, only doubly clamped nanowires were investigated. These resonators were operated by magneto motive actuation, the principle of which is shown in Figure 7. The conducting actuator was positioned in a static magnetic field, and the current through the actuator causes a Lorentz force to bring the device into motion [23, 24]. It is one of the most popular actuation mechanisms for NEMS devices [25].

3. RESULTS AND DISCUSSION

3.1. Nanowire crystallography

There are several methods available to produce tungsten nanowires. However, none of the techniques is able to yield a self-organised array of the single crystalline tungsten nanowires except the method presented here.

Figure 2(a) shows an array of tungsten nanowires embedded in the NiAl matrix. In order to establish whether they are single crystalline as well as determine the growth direction of the two eutectic phases (NiAl and W) and their interfacial planes, orientation imaging microscopy (OIM) was used. EBSD patterns taken from the NiAl matrix and the W nanowires at different locations of the sample are depicted in Figure 2(b). First of all, the identity of the patterns from the NiAl matrix shows that the matrix is single crystalline. Also, the patterns obtained from different nanowires show well-defined Kikuchi lines, proving that they are single crystalline. Moreover, the symmetry and parallelism of the patterns indicate that the nanowires have the same crystallographic orientation, even azimuthally. This practically proves that this method surpasses the drawbacks of the other available methods and is capable of yielding self-organised arrays of the single crystalline tungsten nanowires.

An interesting aspect of directionally solidified eutectics is a preferred crystallographic orientation relationship between the phases. The existence of such specific crystallographic relationships is ascribed to the minimisation of the interface energy between the phases. Cantor [26] has reviewed the evidence for the development of special crystallographic relationships during directional solidification of eutectic alloys and shown that behaviours ranging from strict epitaxial to completely independent growth can occur.

The crystallographic orientation relationship was found to be cube-on-cube, which is characteristic for eutectic alloys containing phases with similar structures, such as NiAl-Cr, Mo, and V. As W also has a BCC structure which is crystallographically identical to the B2 ordered structure of NiAl, they also adopt identical growth textures and form a unique orientation relationship.

3.2. Flexibility

As a qualitative test of the mechanical properties of the tungsten nanowires, bending with a micromanipulator was carried out. The sequence of images (Figures 8(a)–8(d)), comprised of snapshots from a video, demonstrates totally elastic bending of a nanowire, even after several load-unload cycles, which is unusual for a brittle material like tungsten. Both high elasticity and ductility of the nanowires observed during bending experiments brought up a necessity for more accurate and quantitative measurements of the mechanical properties which are described in the following sections.

3.3. Young's modulus of nanowires by static bending

A singly clamped tungsten nanowire prepared by the FIB technique is shown in Figure 9. An example for the analysis of lateral positioned nanowires by lateral force microscopy (LFM) is presented in Figure 10. The singly clamped nanowire (see Figure 9) is scanned at different points along the nanowire and lateral deflection of the AFM cantilever is recorded. Figure 10(b) shows three selected line scans separated by about 300 nm. It can clearly be seen that the lateral deflection, and thus the applied force increases when scanning approximate the anchor point, and that the nanowire is released after stronger bending.

Consequently, as expected the stiffness (spring constant) of the nanowire increases with decreased distance to the anchor point, that is, with shorter nanowires. The stiffness value is used to calculate the Young's modulus. A major difficulty in LFM, however, is the accurate determination of the

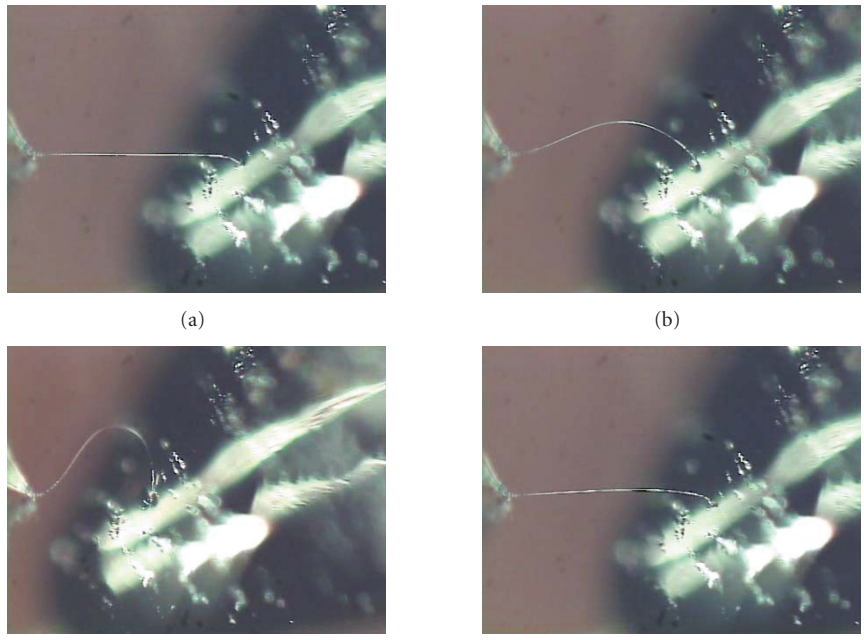

Figure 8: Series of optical images showing the flexibility of tungsten nanowires.

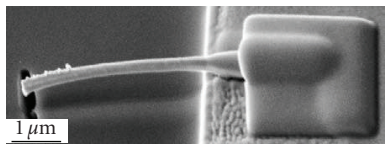

Figure 9: Typical singly clamped lateral aligned tungsten nanowire prepared by FIB on SiO_2/Si substrates with Au pads.

lateral force in Figure 10(b), since the torsional lattice constant of the AFM cantilever cannot be determined with the required accuracy. In contrast, the vertical bending lattice constant of the AFM cantilevers can be obtained with much higher accuracy (e.g., from the resonant frequency), the application of force-displacement curves is much more reliable for the determinations of the Young's modulus. Figure 11 shows the force-displacement curves on the same tungsten nanowire. Similar to the LFM analysis, the stiffness k_{eff} of the system can be determined from the slope in Figure 11(b). The lattice constant k_{NW} of the tungsten nanowire is

$$k_{\text{NW}} = \frac{k_{\text{eff}}\, k_{\text{cantilever}}}{k_{\text{eff}} - k_{\text{cantilever}}}, \tag{4}$$

with the spring constant $k_{\text{cantilever}}$ of the silicon cantilever. Finally, the Young's modulus of the tungsten nanowire is given by

$$E = \frac{4L^3}{3\pi R_{\text{NW}}^4} k_{\text{NW}}. \tag{5}$$

The determined values in dependence on the position on the nanowire are shown in Figure 12. For this nanowire, an average Young's modulus of $E_0 = 332$ GPa was extracted. The analysis of several nanowires results in an average Young's modulus of $E_0 = 362 \pm 62$ GPa, which is very close to the bulk value of $E_0 = 355$ GPa [27]. Nanowires prepared by the e-beam-based technology had a slightly smaller value, however, this difference is within the accuracy of the measurements. As a consequence, nanowires down to 100 nm diameter exhibit a Young's modulus, which does not show dependence on the diameter and is not different from the bulk value.

3.4. Young's modulus from resonant oscillating nanowires

In the case of oscillating nanowires, the Young's modulus is calculated from the measured resonant frequency of magnetomotively driven, doubly clamped nanowires as described in Section 2.5.2. Figure 13 shows the resonant curve of a nanoresonator (insert) prepared by FIB-contacting of a tungsten nanowire.

The calculated Young's modulus (E~450 GPa) for this structure strongly differs from the bulk value. Generally, the dynamic measurements yield to higher values for the Young's modulus (400–650 GPa). The main reason for this phenomenon is the high contamination during the processing. All the resonator bridges were prepared by the FIB technique, and Auger electron spectroscopic investigations have shown that these nanowires were higher contaminated with carbon and traces of Pt then the singly-clamped nanowires used for the static measurements. As a consequence, the highest values for the apparent Young's modulus were obtained for the nanowires with the highest contamination level. These contaminations affect the resonant behaviour of the nanowire by simple mass loading Δm according to

$$\Delta f_{\text{res}} = -\frac{1}{2} f_{\text{res}} \frac{\Delta m}{m}, \tag{6}$$

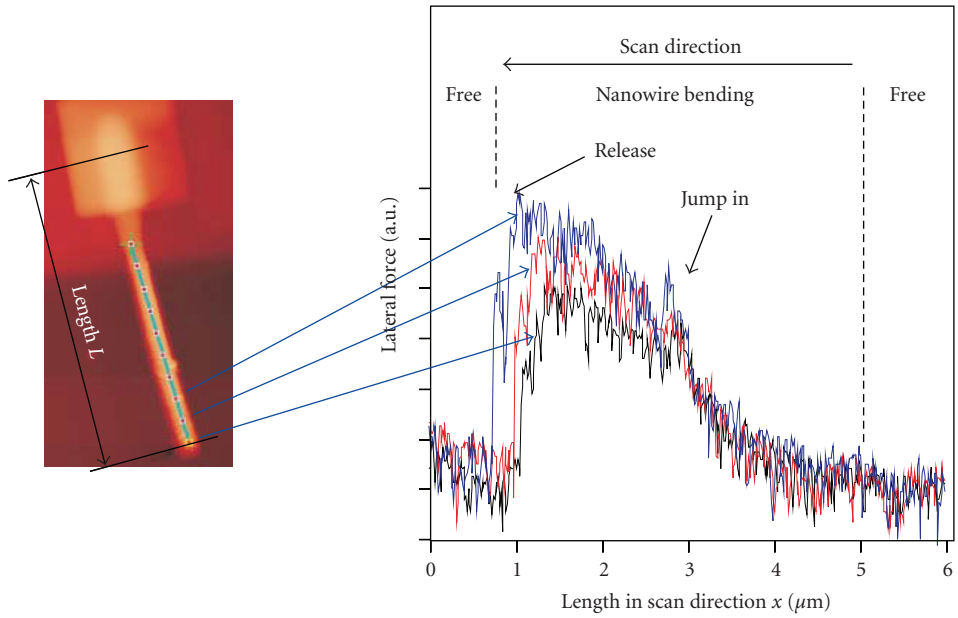

Figure 10: LFM analysis on a tungsten nanowire: (a) AFM topography image, (b) 3 selected LFM line scans, recorded crossing the marked points on the nanowire.

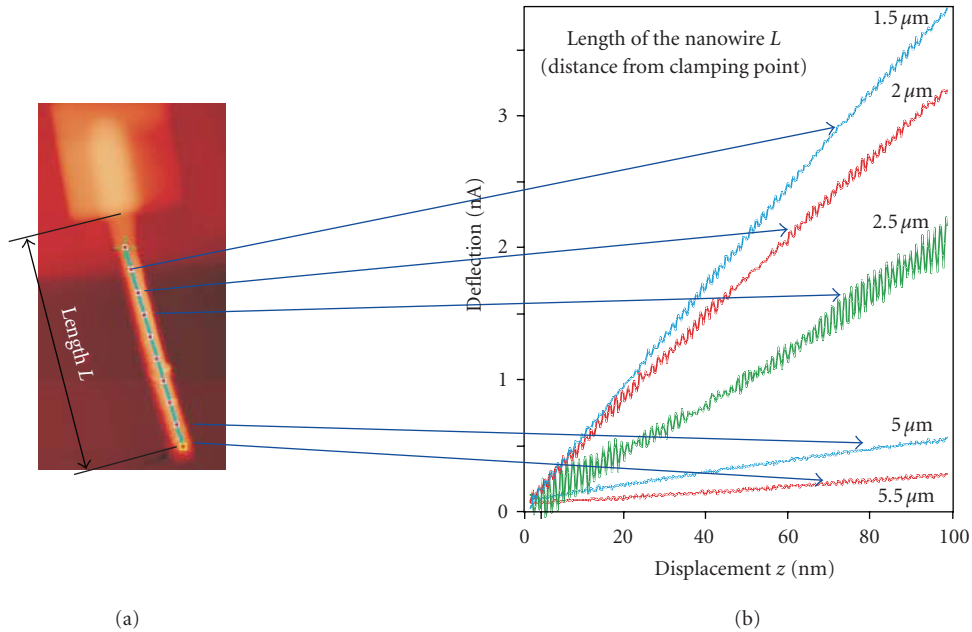

Figure 11: Force displacement analysis of a W nanowire: (a) AFM topography image, (b) selected *F*-*z* curves, recorded crossing the marked points on the nanowire.

or by introducing additional strain, which also alters the resonant frequency [28–30]. Consequently, the apparent Young's modulus is not representative for the pure tungsten nanowire but an effective value for the processed nanoresonator. This observation underlines the importance of controlling the processing technologies, the nanowire surfaces, and the environment with highest accuracy while maintaining absolute cleanliness. On the other hand, this phenomenon gives rise to an attractive possibility of using nanowires as highly sensitive sensors [31]. For further qualitative analysis of this effect, two coupled resonators on the same nanowire were investigated (Figure 14).

After bending of a single tungsten nanowire, the original resonator with a resonant frequency of f_{res} = 117 kHz

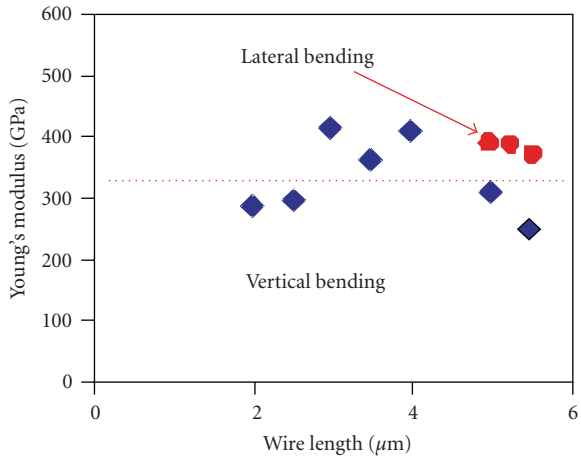

FIGURE 12: Calculated values for the Young's modulus of tungsten nanowires in dependence on the measurement point. The dashed line represents the average value from all measurements.

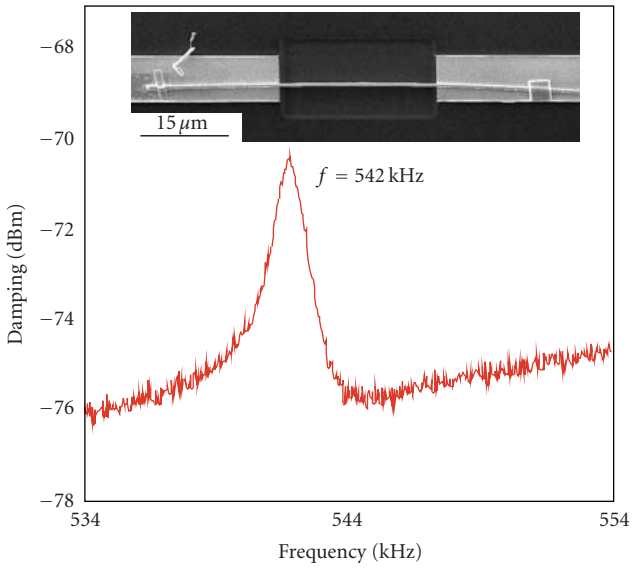

FIGURE 13: Resonance curve of a tungsten nanowire measured by the magnetomotive principle.

(I) splits into two resonators with each with its own resonant frequency (II). After a long-term exposure of the nanowires to air, these two resonant frequencies shift further to higher values (III) indicating a modified structure. Auger electron spectroscopy showed an increased amount of oxygen and carbon on the nanowire surface demonstrating again the high sensitivity of the properties of nanowires to surface modifications. Thus, in contrast to the almost constant behaviour in static bending experiments, contamination and oxidation have a strong influence on the resonant oscillation behaviour of the nanowire, which leads one to expect a discontinuous surface film. The quantification of the influence of these additional surface layers on the mechanical properties of the nanowires and the development of a corresponding analytical model is the subject of the ongoing studies.

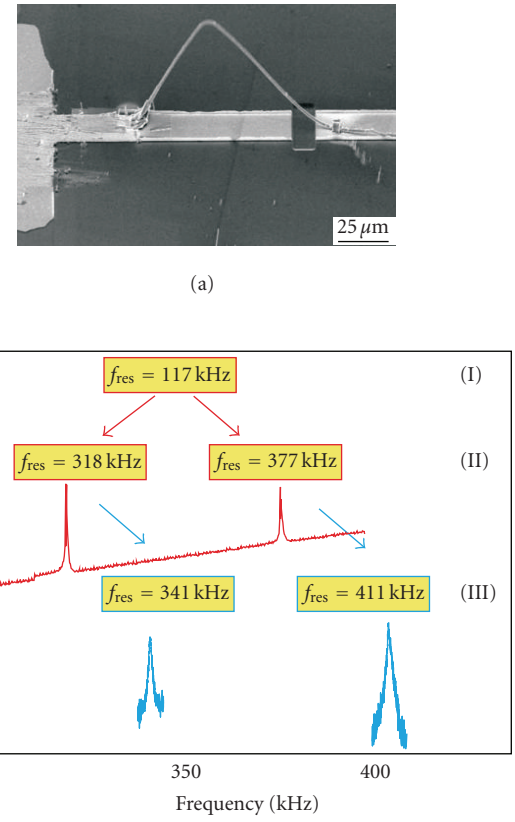

FIGURE 14: (a) Bended, doubly clamped tungsten nanowire resonator and (b) corresponding resonant curves: (I) single resonant frequency before bending, (II) two resonant peaks after bending, and (III) two shifted resonant peaks after 2 months exposure to air.

4. SUMMARY

In this study, single crystalline tungsten nanowires were grown by directional solidification of NiAl-W alloys and were chemically released. Single crystallinity and parallel crystallographic orientation were proven by EBSD. These nanowires were further processed to realise freestanding structures for mechanical characterisation. By different mechanical analysis techniques, it was shown that single crystalline tungsten nanowires with diameters down to 100 nm exhibit a Young's modulus, which is comparable to the bulk value. In bending experiments, these tungsten nanowires have shown a high stability. However, particularly the analysis of resonant nanowire structures revealed that the mechanical properties can be drastically altered by the processing technology and the exposure to the ambient environment. In contrast to semiconducting nanowires such as ZnO, the effective Young's modulus increases. These observations have a high impact on the design of nanowire-based nanomechanical devices. The increased effective Young's modulus is the consequence of the observed contamination and the formation of a surface oxide on the tungsten wire, which alters the geometry as well as the internal strain. A quantitative analysis of this effect will be the subject of future investigations.

ACKNOWLEDGMENTS

The financial support of the DFG through the projects CI 148/2 and HA 3118/4-2 within the frame of the priority programme SPP 1165 "Nanowires and Nanotubes, from controlled synthesis to function" and AM 105/1 within the frame of the priority programme SPP 1157 "Integrierte Elektrokeramische Funktionsstrukturen" is gratefully acknowledged.

REFERENCES

[1] P. Villars and L. D. Calvert, *Pearson's Handbook of Crystallographic Data for Intermetallic Phases*, American Society for Metals, Metals Park, Materials Park, Ohio, USA, 1985.

[2] J. B. Lambert and J. J. Rausch, "Refractory metals and alloys," in *Metals Handbook Vol. 2. Properties and Selection: Nonferrous Alloys and Special-Purpose Materials*, pp. 558–585, ASM International, Materials Park, Ohio, USA, 10th edition, 1990.

[3] A. V. Melechko, V. I. Merkulov, T. E. McKnight, et al., "Vertically aligned carbon nanofibers and related structures: controlled synthesis and directed assembly," *Journal of Applied Physics*, vol. 97, no. 4, Article ID 041301, 39 pages, 2005.

[4] D.-L. Chen and T.-C. Chen, "Mechanical properties of Au nanowires under uniaxial tension with high strain-rate by molecular dynamics," *Nanotechnology*, vol. 16, no. 12, pp. 2972–2981, 2005.

[5] H. S. Park and J. A Zimmerman, "Modelling inelasticity and failure in gold nanowires," *Physical Review B*, vol. 72, no. 5, Article ID 054106, 9 pages, 2005.

[6] Y. S. Kwon, A. A. Gromov, A. P. Ilyin, et al., "Features of passivation, oxidation and combustion of tungsten nanopowders by air," *International Journal of Refractory Metals and Hard Materials*, vol. 22, no. 6, pp. 235–241, 2004.

[7] B. Wu, A. Heidelberg, J. J. Boland, J. E. Sader, X. Sun, and Y. Li, "Microstructure-hardened silver nanowires," *Nano Letters*, vol. 6, no. 3, pp. 468–472, 2006.

[8] M. D. Uchic, D. M. Dimiduk, J. N. Florando, and W. D. Nix, "Sample dimensions influence strength and crystal plasticity," *Science*, vol. 305, no. 5686, pp. 986–989, 2004.

[9] Z. L. Wang, "Mechanical properties of nanowires and nanobelts," in *Dekker Encyclopedia of Nanoscience and Nanotechnology*, pp. 1773–1786, Marcel Dekker, New York, NY, USA, 2004.

[10] A. W. Hassel, B. Bello-Rodriguez, S. Milenkovic, and A. Schneider, "Electrochemical production of nanopore arrays in a nickel aluminium alloy," *Electrochimica Acta*, vol. 50, no. 15, pp. 3033–3039, 2005.

[11] A. W. Hassel, A. J. Smith, and S. Milenkovic, "Nanostructures from directionally solidified NiAl-W eutectic alloys," *Electrochimica Acta*, vol. 52, no. 4, pp. 1799–1804, 2006.

[12] S. Milenkovic, A. J. Smith, and A. W. Hassel, "Single crystalline Mo nanowires, nanowire arrays and nanopore arrays in nickel-aluminum," *Journal of Nanoscience and Nanotechnology*. In press.

[13] S. Brittman, A. J. Smith, S. Milenkovic, and A. W. Hassel, "Copper nanowires and silver micropit arrays from the electrochemical treatment of a directionally solidified silver-copper eutectic," *Electrochimica Acta*, vol. 53, no. 2, pp. 324–329, 2007.

[14] S. Milenkovic, A. W. Hassel, and A. Schneider, "Gold nanostructures by directional solid-state decomposition," *Gold Bulletin*, vol. 39, no. 4, pp. 185–191, 2006.

[15] Y. Chen, S. Milenkovic, and A. W. Hassel, "Arrays of isooriented gold nanobelts," *Nano Letters*, vol. 8, no. 2, pp. 737–742, 2008.

[16] S. Milenkovic, A. W. Hassel, and A. Schneider, "Effect of the growth conditions on the spatial features of Re nanowires produced by directional solidification," *Nano Letters*, vol. 6, no. 4, pp. 794–799, 2006.

[17] A. W. Hassel, S. Milenkovic, U. Schürmann, et al., "Model systems with extreme aspect ratio, tuneable geometry, and surface functionality for a quantitative investigation of the lotus effect," *Langmuir*, vol. 23, no. 4, pp. 2091–2094, 2007.

[18] L. Philippe, I. Peyrot, J. Michler, A. W. Hassel, and S. Milenkovic, "Yield strength of monocrystalline rhenium nanowires," *Applied Physics Letters*, vol. 91, no. 11, Article ID 111919, 3 pages, 2007.

[19] H. Bei, S. Shim, E. P. George, M. K. Miller, E. G. Herbert, and G. M. Pharr, "Compressive strengths of molybdenum alloy micro-pillars prepared using a new technique," *Scripta Materialia*, vol. 57, no. 5, pp. 397–400, 2007.

[20] M. Niebelschütz, V. Cimalla, O. Ambacher, T. Machleidt, J. Ristic, and E. Calleja, "Electrical performance of gallium nitride nanocolumns," *Physica E*, vol. 37, no. 1-2, pp. 200–203, 2007.

[21] W. I. Jang, C. A. Choi, M. L. Lee, C. H. Jun, and Y. T. Kim, "Fabrication of MEMS devices by using anhydrous HF gasphase etching with alcoholic vapour," *Journal of Micromechanics and Microengineering*, vol. 12, no. 3, pp. 297–306, 2002.

[22] W. Weaver Jr., S. P. Timoshenko, and D. H. Young, *Vibration Problems in Engineering*, John Wiley & Sons, New York, NY, USA, 5th edition, 1990.

[23] A. N. Cleland and M. L. Roukes, "Fabrication of high frequency nanometer scale mechanical resonators from bulk Si crystals," *Applied Physics Letters*, vol. 69, no. 18, pp. 2653–2655, 1996.

[24] K. Brückner, V. Cimalla, F. Niebelschütz, et al., "Strain- and pressure-dependent RF response of microelectromechanical resonators for sensing applications," *Journal of Micromechanics and Microengineering*, vol. 17, no. 10, pp. 2016–2023, 2007.

[25] K. L. Ekinci and M. L. Roukes, "Nanoelectromechanical systems," *Review of Scientific Instruments*, vol. 76, no. 6, Article ID 061101, 12 pages, 2005.

[26] B. Cantor, "Interphase interfaces," in *Grain Boundary Structure and Properties*, G. A. Chadwick and D. A. Smith, Eds., Academic Press, London, UK, 1976.

[27] D. Mende and G. Simon, *Physik—Gleichungen und Tabellen*, VEB Fachbuchverlag, Leipzig, Germany, 1986.

[28] V. Cimalla, F. Will, K. Tonisch, et al., "Nanoelectromechanical devices for ultra sensitive sensors," *Sensors and Actuators B*, vol. 126, no. 1, pp. 24–34, 2006.

[29] V. Cimalla, Ch. Föerster, F. Will, et al., "Pulsed mode operation of strained microelectromechanical resonators in air," *Applied Physics Letters*, vol. 88, no. 25, Article ID 253501, 3 pages, 2006.

[30] S. S. Verbridge, J. M. Parpia, R. B. Reichenbach, L. M. Bellan, and H. G. Craighead, "High quality factor resonance at room temperature with nanostrings under high tensile stress," *Journal of Applied Physics*, vol. 99, no. 12, Article ID 124304, 8 pages, 2006.

[31] X. M. H. Huang, M. Manolidis, S. C. Jun, and J. Hone, "Nanomechanical hydrogen sensing," *Applied Physics Letters*, vol. 86, no. 14, Article ID 143104, 3 pages, 2005.